Proton dominance in the $2_2^+ \rightarrow 0_1^+$ transition of $N = Z \pm 2$ nuclei around ^{28}Si

Yoshiko Kanada-En'yo
Department of Physics, Kyoto University, Kyoto 606-8502, Japan
(Received 20 April 2011; revised manuscript received 1 July 2011; published 22 August 2011)

$E2$ transitions in ^{30}Si are investigated in relation to intrinsic deformations based on a method of antisymmetrized molecular dynamics. By comparing $E2$ transition strengths in the mirror nuclei ^{30}Si and ^{30}S, transition matrix amplitudes M_p and M_n for protons and neutrons are discussed in mirror analysis. Particular attention is paid to the M_n/M_p ratio in the transition from the 2_2^+ state to the 0_1^+ state. The M_n/M_p ratio in ^{26}Mg and ^{26}Si is also investigated. It is found that the proton dominance in the transition $2_2^+ \rightarrow 0_1^+$ in ^{30}Si and ^{26}Si originates in the oblate trend of the $Z = 14$ proton structure.

DOI: 10.1103/PhysRevC.84.024317 PACS number(s): 23.20.Lv, 21.10.Ky, 27.30.+t, 02.70.Ns

I. INTRODUCTION

Nuclear systems often show intrinsic quadrupole deformations. In many nuclei except for shell-closed nuclei, normal deformations are found in the ground bands. Shell effects are essential for the deformations as described by the Nilsson model, and therefore, a variety of shapes appear depending on the mass number particular in mid-shell nuclei. In $Z = N$ nuclei in the sd-shell region, a nuclear shape rapidly changes as a function of $Z = N$ reflecting the proton-neutron coherent shell effects in deformed systems. For instance, the prolate ground band in ^{20}Ne and the oblate one in ^{28}Si are known. These shapes are easily understood from the shell effects in the Nilsson model, where the $Z = N = 10$ and $Z = N = 14$ shell gaps appear in the prolate and the oblate deformations, respectively.

For $Z \neq N$ nuclei, deformation phenomena are not as simple as in $Z = N$ nuclei. If the shell effect for proton orbits and that for neutron ones compete with each other, the proton shape can be affected by the neutron structure, or decoupling between proton and neutron deformations may occur. The latter case might be possible in light-mass nuclei and it may be observed in the quadrupole transition properties such as the ratio of the neutron transition matrix amplitude to the proton one (the so-called M_n/M_p ratio). Such a decoupling between proton and neutron shapes has been suggested, for instance, in ^{16}C, for which an enhanced M_n/M_p ratio, i.e., neutron dominance, was observed in the ground-band transition [1]. The neutron dominance was described by the oblate proton and prolate neutron shapes [2,3]. One of the reasons for the characteristic structure of ^{16}C is that a $Z = 6$ system favors an oblate proton deformation while an $N = 10$ nucleus has the prolate trend of the neutron deformation because of each shell effect of the proton and neutron parts. To clarify the oblate tendency of the proton structure in ^{16}C, a possible $K = 2$ side band and its transition properties should be experimentally observed. In general, such a nucleus having oblate proton and prolate neutron structures may show an isovector triaxiality. If this is the case, in addition to the $K = 0$ band, a $K = 2$ side band is constructed with the rotation around the symmetric axis of the prolate neutron part. Since the proton contribution should be dominant while the neutron contribution is minor for this rotation, the transition from the 2_2^+ state in the $K = 2$ band to the ground state may show the proton dominance resulting in a small M_n/M_p ratio. Although the $K = 2$ side band was theoretically suggested, the 2_2^+ state in ^{16}C has not been experimentally confirmed yet, unfortunately. ^{10}C is another candidate for the nuclei with the isovector triaxiality [2,4], but the transition strength from the 2_2^+ state to the 0_1^+ state has not yet been measured.

A similar situation of the isovector triaxiality is expected in $Z = 14$ nuclei, i.e., Si isotopes, because the oblate proton structure is favored due to the $Z = 14$ shell effect. Let us consider deformations of ^{26}Si and ^{30}Si. From the negative sign of the Q moments for the 2_1^+ states in the $Z = N = 12$ and $Z = N = 16$ systems, the prolate trend of the neutron structure is expected in $N = 12$ and $N = 16$ systems. Considering the prolate tendency of the neutron part, the isovector triaxiality in ^{26}Si and ^{30}Si would be possible and it might lead to the proton dominance in the $2_2^+ \rightarrow 0_1^+$ transition resulting in a small M_n/M_p ratio. For ^{26}Si and ^{30}Si, the M_n/M_p ratios for the $2_2^+ \rightarrow 0_1^+$ transition as well as the $2_1^+ \rightarrow 0_1^+$ was experimentally determined by mirror analysis [5,6] and inelastic scattering data [7]. The reported values of the M_n/M_p ratio in the $2_2^+ \rightarrow 0_1^+$ are 0.50 ± 0.07 and 0.52 ± 0.03 for ^{26}Si and ^{30}Si, respectively, and they indicate the proton dominance. The data of neutron and proton transition matrices, M_n and M_p, in this mass region are qualitatively reproduced by shell model calculations [8] and they have been discussed in relation to effective charges coming from core polarization [8,9]. The proton dominance in the $2_2^+ \rightarrow 0_1^+$ of ^{26}Si was discussed also in relation to the γ softness in the calculations based on the quadrupole collective Hamiltonian [10].

Our aim is to understand the properties of proton and neutron transition matrices from the viewpoint of deformations of proton and neutron parts. In particular, the proton dominance in the $2_2^+ \rightarrow 0_1^+$ is a focusing feature which might be interpreted in connection with decoupling of proton and neutron shapes. To this aim, we apply a theoretical approach of antisymmetrized molecular dynamics (AMD). The AMD has been successfully applied to the study of structures of p-shell and sd-shell nuclei [11–13]. The present method of AMD calculations is the same as those used for investigation

of deformation phenomena in ^{28}Si, ^{24}Ne, ^{22}O, and ^{20}C [14] and those in C isotopes [2].

Applying the AMD method, we investigate the transition properties of ^{30}Si. Assuming the mirror symmetry, the calculated proton and neutron transition matrix amplitudes are compared with the data evaluated by the observed $E2$ transition strength for ^{30}Si and ^{30}S, and they are discussed in connection with proton and neutron deformations. Transition properties in ^{26}Mg and ^{26}Si are also discussed. The proton dominance in the transition $2_2^+ \to 0_1^+$ for ^{10}C and ^{16}C is also shown as well as that for Si isotopes.

The paper is organized as follows. In the next section, the formulation of the present calculation is explained. In Sec. III, the results for ^{30}Si and ^{30}S and those for ^{26}Mg and ^{26}Si are shown and the proton dominance of $2_2^+ \to 0_1^+$ in ^{30}Si and ^{26}Si is discussed. The proton dominance in ^{10}C and ^{16}C is shown in Sec. IV. In Sec. V, a summary is given.

II. FORMULATION

Here we briefly explain the formulation of the present calculations. Details of the formulation of AMD methods for nuclear structure study are explained in Refs. [11–13]. The method of the present calculations is basically same as that in Refs. [11,14].

An AMD wave function $\Phi_{\rm AMD}$ for a system with the mass number A is given by a single Slater determinant of Gaussian wave packets as

$$\Phi_{\rm AMD}(\mathbf{Z}) = \frac{1}{\sqrt{A!}}\mathcal{A}\{\varphi_1, \varphi_2, \ldots, \varphi_A\}, \tag{1}$$

where the ith single-particle wave function is written as

$$\varphi_i = \phi_{\mathbf{X}_i}\chi_i\tau_i, \tag{2}$$

$$\phi_{\mathbf{X}_i}(\mathbf{r}_j) \propto \exp\left\{-\nu\left(\mathbf{r}_j - \frac{\mathbf{X}_i}{\sqrt{\nu}}\right)^2\right\}, \tag{3}$$

$$\chi_i = \left(\frac{1}{2} + \xi_i\right)\chi_\uparrow + \left(\frac{1}{2} - \xi_i\right)\chi_\downarrow. \tag{4}$$

Here the isospin function τ_i is fixed to be up (proton) or down (neutron). The orientation of intrinsic spin ξ_i is also fixed to be $1/2$ or $-1/2$ in the present calculations as done in Refs. [11,14]. The width parameter for the Gaussian wave packet is taken to be $\nu = 0.15$ fm^{-2} which is the optimum value for ^{28}Si used in Ref. [14]. The spatial part, $\phi_{\mathbf{X}_i}$, is written by a Gaussian wave packet localized at the certain position $\mathbf{X}_i$ in the phase space. Then, the AMD wave function is expressed by $\{\mathbf{X}_i\}$ which indicate the Gaussian centers for all the single-particle wave functions and are treated as the independent complex variational parameters.

We perform energy variation for a parity eigenstate, $P^\pm\Phi_{\rm AMD} \equiv \Phi^\pm_{\rm AMD}$, projected from an AMD wave function by means of the frictional cooling method [11]. We consider the AMD wave function obtained by the energy variation as an intrinsic state, and total-angular-momentum projection (P^J_{MK}) is performed after the variation to calculate such observables as energies and transition strengths. The K mixing is incorporated in the total-angular-momentum projection for nonzero J states.

As shown later, two local minimum solutions are obtained in the energy variation for the $Z = 14$ systems. The two minima almost degenerate to each other and may correspond to shape coexistence phenomena as already discussed in the $N = 14$ systems [14]. Comparing the calculated structure properties such as transition strengths with the experimental data, we assign one of two minima to the intrinsic state of the ground band.

By using the obtained wave functions, we calculate the transition matrix amplitudes M_p and M_n for proton and neutron, respectively, and also the $E2$ transition strengths. They are defined as follows:

$$M_p = \langle f||P(t_z = 1/2)r^2Y^2_\mu||i\rangle, \tag{5}$$

$$M_n = \langle f||P(t_z = -1/2)r^2Y^2_\mu||i\rangle, \tag{6}$$

$$B(E2) = \frac{e^2}{2J_i + 1}M_p^2. \tag{7}$$

Here $P(t_z = \pm 1/2)$ are the isospin projection operators for protons and neutrons.

III. RESULTS

A. Effective interaction

The effective nuclear interactions adopted in the present work consist of the central force, the spin-orbit force, and the Coulomb force. We adopt the MV1 force [15] as the central force. The MV1 force contains a zero-range three-body force in addition to the two-body interaction. For interaction parameters, we use the same parameter set as that in Ref. [14]. Namely, the MV1 force (case 1) with the parameters $b = 0$, $h = 0$, and $m = 0.62$ is used. For the spin-orbit force, the two-range Gaussian form of the G3RS force [16] is adopted. The strengths of the spin-orbit force are $u_I = -u_{II} = 2800$ MeV. These strengths were adjusted to reproduce energy levels of ^{28}Si in Ref. [14].

B. ^{30}Si and ^{30}S

After the energy variation for parity projected AMD wave functions, two local minimum solutions (A) and (B) are obtained for ^{30}Si. The state (A) shows a smaller deformation as $(\beta_p, \gamma_p) = (0.18, 0.01\pi)$ and $(\beta_n, \gamma_n) = (0.20, 0.00\pi)$ and the state (B) has a larger deformation as $(\beta_p, \gamma_p) = (0.35, 0.00\pi)$ and $(\beta_n, \gamma_n) = (0.26, 0.00\pi)$. Here the definition of the quadrupole deformation parameters (β_p, γ_p) for proton density distribution and (β_n, γ_n) for a neutron one is given in Ref. [4].

After the angular momentum projection, the energy levels are obtained from the states (A) and (B) (Fig. 1). The bands constructed from two intrinsic states, (A) and (B), almost degenerate. As shown later, the band (A) shows good agreements with experimental data such as the Q moment and $E2$ transition strengths for the ground band, and therefore, we can assign the band (A) to the experimental ground band. The band (B) might correspond to the excited band, but the excitation energy seems to be underestimated in

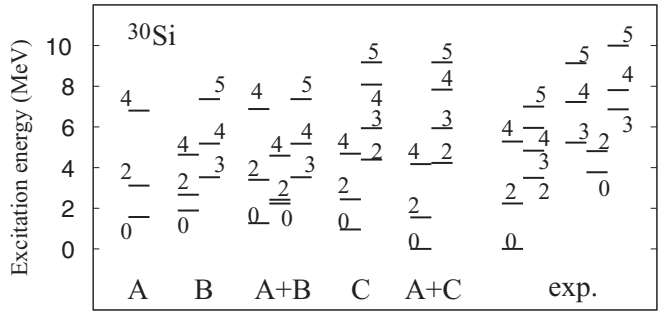

FIG. 1. Energy levels of ^{30}Si for positive parity states. The calculated levels are obtained by the projection from the state (A), the state (B), the superposition (A + B), the state (C), and the superposition (A + C). The energies are measured from the 0^+_1 calculated with (A + C). The experimental levels are the positive parity bands observed by the gamma-ray measurements in Ref. [17].

the present calculation. Because of this underestimation, the energy levels calculated by superposition of (A) and (B) show the band-mixing feature around $J \sim 2$ which is inconsistent with the experimental data. Since our interest is in the transition properties of the ground band and its side band, we consider the state (A) for the ground band and omit the mixing with the state (B) in the following discussions.

Experimentally, the $E2$ transition strengths were measured up to high-spin states, and the $K^\pi = 2^+$ side band by the $K^\pi = 0^+$ ground band was identified [17]. In the present calculation, no $K^\pi = 2^+$ side band member is obtained from the band (A) because of the prolate intrinsic shape of the state (A). Owing to the $Z = 14$ shell gap in the oblate deformation, it is naturally expected that ^{30}Si may be soft against γ deformation toward the oblate region. Therefore, we construct another intrinsic state (C) by the alternative energy variation where we vary the single-particle neutron wave functions but freeze the proton configuration so that it has the same proton structure as that of the oblate ground state of ^{28}Si. It corresponds to the energy variation with the constraint of the oblate proton structure. Thus obtained state (C) has an triaxial neutron structure of $(\beta_n, \gamma_n) = (0.21, 0.15\pi)$ with the oblate proton deformation of $(\beta_p, \gamma_p) = (0.27, 0.28\pi)$. The single-particle energy levels in the intrinsic wave functions for the states (A) and (C) are shown in Fig. 2 . The derivation of the single-particle energies of AMD

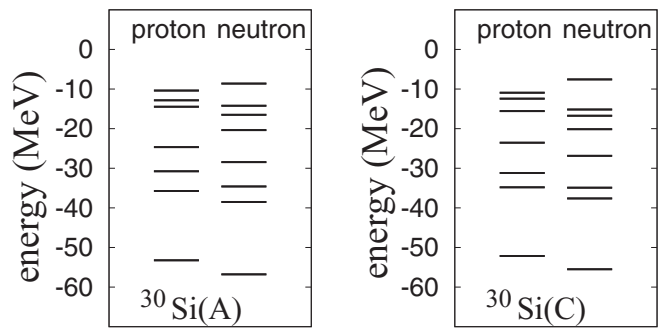

FIG. 2. Single-particle energies in the intrinsic wave functions ^{30}Si(A) and ^{30}Si(C).

wave functions is described, for example, in Refs. [13,18]. In the state (C), the single-particle energy spectra are consistent with those for oblate systems where the $N = 14$ shell gap is clearly seen, while the $N = 14$ shell gap vanishes in the state (A).

After the angular momentum projection, the $K^\pi = 0^+$ and the $K^\pi = 2^+$ side bands are generated from the intrinsic state (C). The absolute energy of the 0^+_1 projected from the state (C) is relatively lower than that from the state (A) even though the intrinsic energy of the state (C) is higher than (A) before the projection. This is because the triaxial state gains more energy than the prolate state in the angular momentum projection. The lower energy of the state (C) than that of the state (A) may support a trend of finite gamma proton configuration. However, we should comment that the state (C) is not necessarily the lowest state in the 0^+_1 projected AMD wave functions though the state (C) is a better solution than the state (A). To get the most relevant state the method of variation after parity and angular momentum projections or the method with β-γ constraint [19] should be applied. However, it is difficult in practice to apply these methods to $A = 30$ nuclei because of computational costs.

We superpose the states (A) and (C) and obtain the energy levels for the ground and side bands. The energy levels calculated by the superposition (A + C) correspond well to the experimental levels for the $K^\pi = 0^+$ and the $K^\pi = 2^+$ bands except for a slightly higher excitation energy for the $K^\pi = 2^+$ band. Considering that the $K^\pi = 2^+$ band members are constructed mainly from the $|K| = 2$ components of the intrinsic state (C) and the ground band can be described by the $K = 0$ states of (C), these bands are considered to be the $K^\pi = 0^+$ and the $K^\pi = 2^+$ side bands projected from the triaxial intrinsic state (C). We here note that the wave functions of the $K^\pi = 0^+$ components of the states (C) and (A) have large overlap with each other. Therefore, an alternative interpretation is possible. Namely, the ground band is regarded as the rotational band of the prolate state (A) and the $K = 2$ side band is the γ vibration band on the top of the prolate state, which is taken into account by the superposition of (A) and (C).

We calculate the quadrupole transition properties by the superposition (A + C) and discuss the neutron and proton contributions based on the mirror analysis. We first show the calculated values of $B(E2)$, the proton transition matrix amplitudes M_p, and electric quadrupole moments Q in ^{30}Si in comparison with the experimental data in Table I. The theoretical values are in good agreement with the experimental data except for the inter-band transition $4^+_2 \to 2^+_1$.

We next discuss the M_n/M_p ratio for the $2^+_1 \to 0^+_1$ and $2^+_2 \to 0^+_1$ transitions. We assume here the mirror symmetry that the neutron transition matrix amplitudes M_n in ^{30}Si are consistent with the proton transition matrix amplitudes M_p in ^{30}S. Then, the experimental M_n values for ^{30}Si are evaluated by $B(E2)$ in ^{30}S. As shown in Table II, the experimental M_n/M_p ratio for $2^+_1 \to 0^+_1$ in ^{30}Si is close to a unit indicating that the proton and neutron parts equally contribute to the ground-band transition. What is striking is that the M_n/M_p ratio for $2^+_2 \to 0^+_1$ is 0.5 in the experimental data. This indicates the dominant proton matrix amplitude, which is about twice the

TABLE I. $E2$ transition strengths of the in-band and inter-band transitions in ^{30}Si. The experimental data are taken from (a) Ref. [20] and (b) Ref. [17].

	Exp.		Cal.	
	$B(E2)$	M_p	$B(E2)$	M_p
Inband ($K=0_1^+$)				
$2_1^+ \to 0_1^+$	8.5 ± 1.1^{a}	14	5.6	12.5
$4_1^+ \to 2_1^+$	$4.5^{+1.5}_{-1.0}{}^{b}$	14	8.7	15.5
Inband ($K=2_1^+$)				
$3_1^+ \to 2_2^+$	$7^{+16}_{-6}{}^{b}$	15	8.5	15.4
$4_2^+ \to 2_2^+$	$4.1^{+3.7}_{-1.8}{}^{b}$	13	7.1	14
$4_2^+ \to 3_1^+$				7.9
$5_1^+ \to 3_1^+$	$4.5^{+2.2}_{-1.4}{}^{b}$	15	7.6	14.5
$5_1^+ \to 4^+2$	$1.3^{+1.4}_{-0.7}{}^{b}$	8.1	4.5	11.1
Inter-band				
$2_2^+ \to 0_1^+$	1.7 ± 0.5^{a}	5.9	1.6	6.6
$2_2^+ \to 2_1^+$	$8.9^{+11}_{-5}{}^{b}$	14	9.1	15.9
$3_1^+ \to 2_1^+$	$3.8^{+2.7}_{-1.3}{}^{b}$	11	2.8	8.8
$4_2^+ \to 2_1^+$	$7.8^{+4.1}_{-1.2}{}^{b}$	18	0.02	0.8
$4_1^+ \to 3_1^+$			4.1	10.6
	Exp.		Cal.	
	Q	μ	Q	μ
2_1^+	-5 ± 6	0.76	-4.1	1.3

neutron one in the transition from the side band to the ground state. The present calculation reproduces this trend of the quenched M_n/M_p ratio, though it much underestimates the M_n value for $2_2^+ \to 0_1^+$ in ^{30}Si. The origin of the dominant proton contribution and the minor neutron one in this transition, $2_2^+ \to 0_1^+$, is understood by the difference between proton and neutron structures. As mentioned before, the side band members are constructed mainly from the $|K|=2$ components of the intrinsic state (C), while the ground band is also approximately written by the $|K|=0$ states projected from the state (C). That is, the 2_2^+ state can be interpreted as the triaxial side band. As we mentioned, the state (C) has the larger triaxiality of the proton shape than the neutron part, and therefore, proton contribution should be dominant but the neutron one is minor in the $2_2^+ \to 0_1^+$.

We should comment again that the $K=0$ components of the triaxial state (C) have large overlaps with those of the prolate state (A). In fact, the overlap between the 0^+ states projected from (A) and (C) is 55%. This is because the deformation parameter γ is not a coordinate but just an expectation value, and two states with different γ values are not orthogonal to each other. Even if a rotational band is constructed by the angular-momentum projection from an intrinsic state, the intrinsic shape is not observable but an interpretation which is useful to interpret the microscopic wave functions projected from the intrinsic state as the rotational band members. Therefore, strictly speaking, it is not easy to clearly distinguish between rotational $K=2$ modes of a static triaxial state and γ-vibrational modes in such the system. Then, we can consider the alternative interpretation for the 2_2^+ state as the γ vibration on the prolate $K=0$ ground band. Again, the proton dominance can be easily understood by the γ vibration of the proton structure. In any case, we can conclude that the proton dominance of the transition $2_2^+ \to 0_1^+$ in ^{30}Si originates in the γ softness of the proton part in the $Z=14$ system, and the difference between proton and neutron structures is essential.

TABLE II. The calculated and theoretical $B(E2)$ values and the proton transition matrix for the transitions $2_2^+ \to 0_1^+$ and $2_1^+ \to 0_1^+$ in ^{30}Si and ^{30}S. The experimental values of the M_n/M_p ratio are evaluated based on the mirror analysis in which M_n of ^{30}Si is assumed to be equal to M_p of ^{30}S. The experimental $B(E2)$ values are taken from Ref. [20] and (c) those evaluated from the life times and branching ratios.

	Exp.			Cal.		
	$B(E2)$	M_p	M_n/M_p	$B(E2)$	M_p	M_n/M_p
$2_1^+ \to 0_1^+$						
^{30}Si	8.5 ± 1.1	15.3	1.1	5.6	12.5	1.2
^{30}S	11^{c}	18		7.6	14.5	
$2_2^+ \to 0_1^+$						
^{30}Si	1.7 ± 0.5	6.9	0.5	1.6	6.6	0.1
^{30}S	0.4^{c}	3		0.02	0.6	

C. ^{26}Mg and ^{26}Si

In this subsection, we discuss the proton dominance in the $2_2^+ \to 0_1^+$ of ^{26}Si in relation to the γ deformation of the proton structure, in a similar way to the mirror analysis of ^{30}Si and ^{30}S. Before discussing the M_n/M_p ratio of ^{26}Si based on the mirror analysis, we first investigate the structure of the ground and excited states of the mirror nucleus ^{26}Mg for which the existing data is richer than for ^{26}Si.

We apply the AMD method to ^{26}Mg. After energy variation for parity projected AMD wave functions, two local minimum solutions (A) and (B) are obtained in ^{26}Mg, similarly to the case of ^{30}Si. The state (A) shows the triaxiality shape $(\beta_p, \gamma_p) = (0.33, 0.08\pi)$ and $(\beta_n, \gamma_n) = (0.22, 0.13\pi)$ with a smaller neutron deformation, while the state (B) has a prolate deformation $(\beta_p, \gamma_p) = (0.33, 0.07\pi)$ and $(\beta_n, \gamma_n) = (0.35, 0.00\pi)$ with a larger neutron deformation. The energy of the intrinsic state (A) degenerates with the state (B) within 0.1 MeV before the angular momentum projection. After the angular-momentum projection, the 0^+ energy projected from the state (A) is 1.1 MeV higher than that obtained from the state (B). In spite of the slightly higher energy of the state (A) than that of the state (B), we tentatively assign the states projected from (A) to the experimental $K^\pi = 0^+$ ground band and its side band $K^\pi = 2_1^+$, because the observed level structure and $E2$ transition strengths for the $K^\pi = 0_1^+$ and $K^\pi = 2_1^+$ band members can be reproduced by the results calculated with the state (A). The state (B) is inconsistent with the experimental

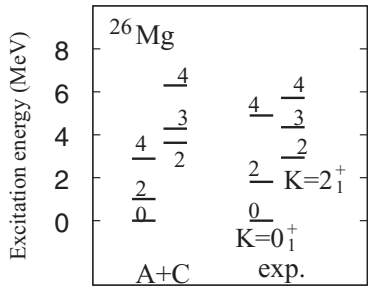

FIG. 3. Energy levels of ^{26}Mg. The calculated levels are obtained by the superposition of the states projected from the states (A) and (C). The experimental levels are the positive parity bands observed by the gamma-ray measurements in Ref. [22].

fact that the $K^\pi = 2^+_1$ side band exists by the ground band, and therefore, it would correspond to an excited $K^\pi = 0^+$ band though it is eventually the lowest in the present calculations. In fact, the state (A) can be the lowest if we tune the interaction parameters, for instance, with $m = 0.62$, $b = h = 0.125$, and $u_I = -u_{II} = 3200$ MeV. Hereafter, we concentrate only on the $K^\pi = 0^+$ band and its $K^\pi = 2^+$ side band constructed from the state (A), and omit the mixing effect of the state (B).

To see the γ softness of the $N = 14$ neutron structure in ^{26}Mg, we construct an intrinsic state (C) by the alternative energy variation that we vary the centers of the single-particle Gaussian wave functions only for protons but freeze the neutron configuration so that it has the same neutron structure as that of the oblate ground state of ^{28}Si. This means energy variation with the constraint of the oblate neutron structure. Thus obtained state (C) of ^{26}Mg has an triaxial proton structure of $(\beta_p, \gamma_p) = (0.32, 0.10\pi)$ with the almost oblate neutron deformation $(\beta_n, \gamma_n) = (0.26, 0.28\pi)$. The state (C) is 2 MeV higher than the state (A) before and after the angular momentum. In Fig. 3, we show the energy levels obtained by the superposition (A + C). The calculated energy levels are in reasonable agreement with the experimental data except for underestimation of the level spacing in the ground band. In the case of ^{26}Mg, the mixing of the state (C) gives minor contributions and the energy levels in the (A + C) calculations are qualitatively the same as those obtained by the single intrinsic state (A) without mixing of the state (C). This indicates that the $K^\pi = 2^+_1$ band can be interpreted as the side band of the $K^\pi = 0^+_1$ ground band constructed from the triaxial shape of state (A).

Let us show the quadrupole transition properties calculated by the superposition (A + C) and discuss the proton and neutron matrix amplitudes based on the mirror analysis. We first show the calculated values of the $B(E2)$ and Q moments of ^{26}Mg in Table III. The present results are in reasonable agreement with the experimental data. Next we discuss the M_n/M_p ratio for the transitions $2^+_1 \to 0^+_1$ and $2^+_2 \to 0^+_1$ in ^{26}Si, shown in Table IV. Here we assume the mirror symmetry that M_n and M_p of ^{26}Si are equal to M_p and M_n of ^{26}Mg, respectively. The experimental values of M_p are obtained from the $B(E2)$ values of ^{26}Si and ^{26}Mg. The experimental M_n/M_p ratio for the ground-band transition $2^+_1 \to 0^+_1$ is 0.94

TABLE III. $E2$ transition strengths for the in-band and inter-band transitions in ^{26}Mg. The experimental data are taken from (a) [21] and (b) [22].

	Exp.		Cal.	
	$B(E2)$	M_p	$B(E2)$	M_p
Inband ($K = 0^+_1$)				
$2^+_1 \to 0^+_1$	13.4 ± 0.4^a	17.5	12.9	17.2
$4^+_2 \to 2^+_1$	14 ± 3^a	24	16.1	25.7
Inband ($K = 2^+_1$)				
$3^+_2 \to 2^+_2$	$9.2^{+7.9b}_{-4.5}$	17	22.5	26.8
$4^+_4 \to 3^+_2$	$5.2^{+6.1b}_{-2.1}$	15	9.5	19.8
Inter-band				
$2^+_2 \to 0^+_1$	0.35 ± 0.07^a	2.8	0.1	1.5
	Exp.		Cal.	
	Q	μ	Q	μ
2^+_1	-13.5 ± 2	0.884	-14.2	0.92

which is close to 1, while that for the $2^+_2 \to 0^+_1$ is 0.5. The quenched M_n/M_p for the transition $2^+_2 \to 0^+_1$ indicates proton dominance. The present calculations reproduce this feature of the proton dominance.

Here we remind the reader that the 2^+_2 state of ^{26}Mg is constructed from the triaxial neutron shape of the state (A). In other words, the 2^+_2 state of the mirror nucleus ^{26}Si is given by the rotation of the triaxial proton shape. Consequently, the proton contribution is dominant in the excitation from the 0^+_1 state to the 2^+_2 state resulting in the small value of M_n/M_p for the transition $2^+_2 \to 0^+_1$ in ^{26}Si.

IV. M_n/M_p RATIOS IN p-SHELL NUCLEI

In the previous section, we discuss the the proton dominance in the transition $2^+_2 \to 0^+_1$ between the side band and the ground band of Si isotopes with $N = Z \pm 2$. The proton

TABLE IV. The calculated and theoretical $B(E2)$ values and the proton transition matrix for the transitions $2^+_2 \to 0^+_1$ and $2^+_1 \to 0^+_1$ in ^{26}Si and ^{26}Mg. The experimental values of the M_n/M_p ratio are evaluated based on the mirror analysis in which M_n of ^{26}Si is assumed to be equal to M_p of ^{26}Mg. The experimental $B(E2)$ values are taken from Ref. [21].

	Exp.			Cal.		
	$B(E2)$	M_p	M_n/M_p	$B(E2)$	M_p	M_n/M_p
$2^+_1 \to 0^+_1$						
^{26}Si	15.4 ± 1.5	18.8	0.94	6.4	12.1	1.4
^{26}Mg	13.4 ± 0.4	17.5		12.9	17.2	
$2^+_2 \to 0^+_1$						
^{26}Si	1.6 ± 0.5	6.0	0.5	1.4	5.6	0.26
^{26}Mg	0.35 ± 0.07	2.8		0.09	1.5	

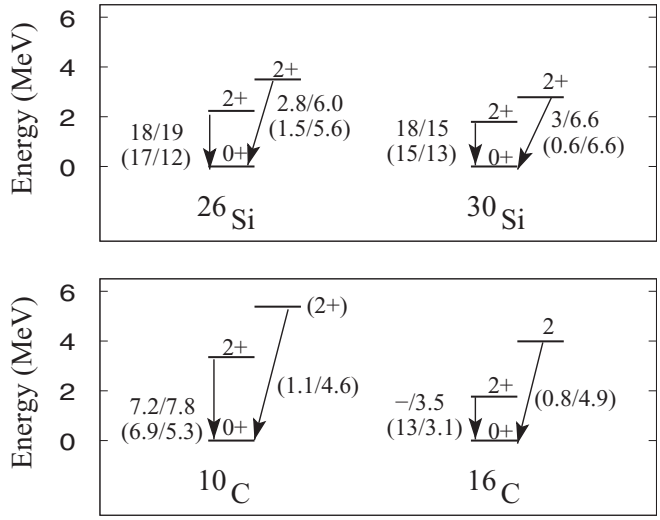

FIG. 4. The experimental energy levels of the 0_1^+, 2_1^+, and 2_2^+ states and M_n/M_p ratios for the $2_1^+ \to 0_1^+$ and $2_2^+ \to 0_1^+$ of ^{26}Si, ^{30}Si, ^{10}C, and ^{16}C [20,21,23,24]. The experimental values of the neutron matrix amplitude (M_n) are deduced from the corresponding $B(E2)$ values of the mirror nucleus. The values in the parentheses are the present calculations.

dominance can be described by the triaxial shape of the proton structure. This feature originates in the oblate trend of the $Z = 14$ proton configuration.

Let us consider the proton dominance in the p-shell nuclei. In C isotopes, the $Z = 6$ proton configuration has the oblate trend as is known in ^{12}C. In fact, the oblate proton and prolate neutron shapes are theoretically suggested in ^{10}C and ^{16}C in the AMD calculations [2]. In these nuclei, the proton dominance in the transition $2_2^+ \to 0_1^+$ is expected as well as ^{26}Si and ^{30}Si. In this section, we refer to the intrinsic structures of ^{10}C and ^{16}C investigated in Ref. [2] and discuss the proton dominance in C isotopes in comparison with Si isotopes. We use the AMD wave functions calculated in the previous work [2].

The experimental and theoretical values of the M_n/M_p ratios are written in Fig. 4, in which the experimental energy levels are drawn. In both nuclei ^{10}C and ^{16}C, the proton structure shows the oblate deformation in spite of the prolate neutron structure. The deformation parameters of the intrinsic state are $(\beta_p, \gamma_p) = (0.41, 0.27\pi)$ and $(\beta_n, \gamma_n) = (0.53, 0.00\pi)$ for ^{10}C, and they are $(\beta_p, \gamma_p) = (0.32, 0.26\pi)$ and $(\beta_n, \gamma_n) = (0.34, 0.00\pi)$ for ^{16}C. This means that the $Z = 6$ proton structure is not so much affected by the neutron structure but it keeps the oblate tendency. As a result, the decoupling between proton and neutron shapes is more remarkable in C isotopes than in Si isotopes. This decoupling is one of the reasons for the enhanced M_n/M_p ratio of the ground-band transition $2_1^+ \to 0_1^+$ in ^{16}C as discussed in Ref. [2]. For the transition $2_2^+ \to 0_1^+$ in ^{10}C and ^{16}C, the calculated M_n/M_p ratio is quenched and it indicates the proton dominance. The suggested proton dominance originates in the oblate proton structure in the $Z = 6$ systems. This is a good analogy to the proton dominance in ^{26}Si and ^{30}Si, which arises from the oblate trend of the $Z = 14$ proton structure.

Experimentally, the M_n/M_p ratio for $2_2^+ \to 0_1^+$ is unknown. Inelastic scatterings of ^{10}C and ^{16}C might be a good probe to evaluate the M_n/M_p ratio.

Note that the shape has large quantum fluctuation in such light systems and it is not observable. Nevertheless, it is helpful to interpret the angular-momentum-projected states in terms of rotation of the intrinsic deformation to get the semiclassical picture of transition properties. Our argument is that the M_n/M_p ratios in C isotopes can be qualitatively understood by the oblate proton and prolate neutron shapes.

V. SUMMARY

$E2$ transitions in ^{30}Si were investigated in relation with the intrinsic deformation. In the calculation of the AMD method, the experimental $B(E2)$ values in the $K^\pi = 0_1^+$ and $K^\pi = 2_1^+$ bands are reproduced by the calculation. Based on mirror analysis, the transition matrix amplitudes M_p and M_n were discussed. Particular attention is paid to the M_n/M_p ratio in the transition from the 2_2^+ state to the 0_1^+ state, whose quenching is experimentally known. The M_n/M_p ratio in ^{26}Mg and ^{26}Si was also investigated. We have shown that the $K^\pi = 2_1^+$ band can be interpreted as the triaxial side band, and the proton contribution is dominant in the transition $2_2^+ \to 0_1^+$. The quenched M_n/M_p, i.e., the proton dominance in $2_2^+ \to 0_1^+$ in ^{30}Si and ^{26}Si, originates in the oblate trend of the $Z = 14$ proton structure. The proton dominance in $2_2^+ \to 0_1^+$ is suggested also in ^{10}C and ^{16}C, where the oblate proton structure is favored.

We should comment that the shape has large quantum fluctuation in light-mass systems and it is not observable. Strictly speaking, the macroscopic picture may be too simple for such systems, and therefore, it is not easy to clearly distinguish between two collective pictures, the rotational mode of a static triaxial state and the γ-vibrational mode. Nevertheless, it is helpful to interpret the angular-momentum-projected states in terms of rotation of the intrinsic deformation to get the semiclassical picture of transition properties. Our argument is that the quenched M_n/M_p ratios in $2_2^+ \to 0_1^+$ of these nuclei can be qualitatively understood by the oblate trend of proton shapes in the prolate neutron structures.

ACKNOWLEDGMENTS

The computational calculations of this work were performed by using the supercomputers at YITP and done in Supercomputer Projects of the High Energy Accelerator Research Organization (KEK). This work was supported by a Grant-in-Aid for Scientific Research from the Japan Society for the Promotion of Science (JSPS). It was also supported by the Grant-in-Aid for the Global COE Program "The Next Generation of Physics, Spun from Universality and Emergence" from the Ministry of Education, Culture, Sports, Science, and Technology (MEXT) of Japan.

[1] Z. Elekes *et al*., Phys. Lett. B **586**, 34 (2004).
[2] Y. Kanada En'yo, Phys. Rev. C **71**, 014310 (2005).
[3] M. Takashina, Y. Kanada En'yo, and Y. Sakuragi, Phys. Rev. C **71**, 054602 (2005).
[4] Y. Kanada En'yo and H. Horiuchi, Phys. Rev. C **55**, 2860 (1997).
[5] T. K. Alexander *et al*., Phys. Lett. B **113**, 132 (1982).
[6] T. K. Alexander *et al*., Phys. Rev. Lett. **49**, 438 (1982).
[7] F. Sciuccati, S. Micheletti, M. Pignanelli, and R. De Leo, Phys. Rev. C **31**, 736 (1985).
[8] B. A. Brown *et al*., Phys. Rev. C **26**, 2247 (1982).
[9] T. K. Alexander, B. Castel, and I. S. Towner, Nucl. Phys. A **445**, 189 (1985).
[10] N. Hinohara and Y. Kanada En'yo, Phys. Rev. C **83**, 014321 (2011).
[11] Y. Kanada En'yo, H. Horiuchi and A. Ono, Phys. Rev. C **52**, 628 (1995); Y. Kanada En'yo and H. Horiuchi, *ibid*. **52**, 647 (1995).
[12] Y. Kanada En'yo and H. Horiuchi, Prog. Theor. Phys. Suppl. **142**, 205 (2001).
[13] Y. Kanada En'yo, M. Kimura, and H. Horiuchi, C. R. Phys. **4**, 497 (2003).
[14] Y. Kanada En'yo, Phys. Rev. C **71**, 014303 (2005).
[15] T. Ando, K. Ikeda, and A. Tohsaki, Prog. Theor. Phys. **64**, 1608 (1980).
[16] N. Yamaguchi, T. Kasahara, S. Nagata, and Y. Akaishi, Prog. Theor. Phys. **62**, 1018 (1979); R. Tamagaki, *ibid*. **39**, 91 (1968).
[17] E. Bitterwolf *et al*., Z. Phys. A **298**, 279 (1980).
[18] A. Dote, H. Horiuchi, and Y. Kanada En'yo, Phys. Rev. C **56**, 1844 (1997).
[19] T. Suhara and Y. Kanada En'yo, Prog. Theor. Phys. **123**, 303 (2010).
[20] M. Shamsuzzoha Basunia, Nucl. Data Sheets **111**, 2331 (2010).
[21] P. M. Endt, J. Blachot, R. B. Firestone, and J. Zipkin, Nucl. Phys. A **633**, 1 (1998).
[22] F. Glatz *et al*., Z. Phys. A **324**, 187 (1986).
[23] J. H. Kelley, C. G. Sheu, J. L. Godwin *et al*., Nucl. Phys. A **745**, 155 (2004).
[24] H. J. Ong *et al*., Phys. Rev. C **78**, 014308 (2008).